THE JOURNAL OF BIOLOGICAL CHEMISTRY VOL. 287, NO. 13, pp. 9722–9730, March 23, 2012

Substrate Binding in Protein-tyrosine Phosphatase-like Inositol Polyphosphatases*[S]

Received for publication, October 19, 2011, and in revised form, November 30, 2011 Published, JBC Papers in Press, December 2, 2011, DOI 10.1074/jbc.M111.309872

Robert J. Gruninger[‡], Selina Dobing[‡], Adam D. Smith[‡], Lisza M. Bruder[‡], L. Brent Selinger[§], Hans-Joachim Wieden[‡], and Steven C. Mosimann[‡1]

From the Departments of [‡]Chemistry and Biochemistry and [§]Biological Sciences, University of Lethbridge, Lethbridge, Alberta, Canada T1K 3M4

Background: PTP-like inositol polyphosphatases hydrolyze *myo*-inositol hexa*kis*phosphate via an ordered pathway.
Results: X-ray structures in complex with substrates and fluorescence binding reveal novel features of the kinetic mechanism.
Conclusion: PTP-like inositol polyphosphatases have a two-step binding mechanism that facilitates specificity and catalysis.
Significance: Structural and binding studies are essential for understanding complex kinetic mechanisms.

Protein-tyrosine phosphatase-like inositol polyphosphatases are microbial enzymes that catalyze the stepwise removal of one or more phosphates from highly phosphorylated *myo*-inositols via a relatively ordered pathway. To understand the substrate specificity and kinetic mechanism of these enzymes we have determined high resolution, single crystal, x-ray crystallographic structures of inactive *Selenomonas ruminantium* PhyA in complex with *myo*-inositol hexa- and penta*kis*phosphate. These structures provide the first glimpse of a *myo*-inositol polyphosphatase-ligand complex consistent with its known specificity and reveal novel features of the kinetic mechanism. To complement the structural studies, fluorescent binding assays have been developed and demonstrate that the K_d for this enzyme is several orders of magnitude lower than the K_m. Together with rapid kinetics data, these results suggest that the protein tyrosine phosphatase-like inositol polyphosphatases have a two-step, substrate-binding mechanism that facilitates catalysis.

myo-Inositol polyphosphates (IPPs)[2] are ubiquitous in nature and are involved in a number of important cellular signaling events (1). *myo*-Inositol 1,2,3,4,5,6-hexa*kis*phosphate (phytic acid, $InsP_6$) is the most abundant cellular IPP and plays a central role in numerous essential cellular processes, including DNA repair, RNA processing, mRNA export, plant development, apoptosis, and bacterial pathogenicity (2–7). Inositol polyphosphatases (IPPases) that degrade IPPs are found throughout nature and have been identified in prokaryotes, protists, fungi, animals, and plants (8–10). IPPases that are able to hydrolyze $InsP_6$ are generically referred to as phytases. To date, four classes of IPPases have been described that are structurally and mechanistically diverse, including histidine acid phosphatases, β-propeller phytases, purple acid phosphatases, and protein-tyrosine phosphatase-like phytases (PTPLPs) (11–13). Each of the IPPase classes catalyze the stepwise removal of one or more phosphates from IPPs. The products generated during the breakdown of a specific IPP are released from the enzyme and serve as substrate for subsequent cycles of hydrolysis. Although the biological function of some of these enzymes is unclear, they have been found in a wide range of bacteria, including plant and human pathogens (14, 15).

PTPLPs are particularly interesting because the stepwise removal of phosphate from IPP substrates occurs in a relatively specific order. They have a protein-tyrosine phosphatase (PTP) fold, including the P-loop or PTP active-site signature sequence ($CX_5R(S/T)$) and utilize a classical PTP reaction mechanism (12–13). Interestingly, these enzymes display no catalytic activity against classical PTP substrates due to several unique structural features that confer specificity for IPPs (12–13, 15–17). The structural basis of IPP binding to a representative PTPLP (PhyAsr; *Selenomonas ruminantium* PhyA) has been investigated by x-ray crystallography using the competitive inhibitor, *myo*-inositol hexasulfate (MIHS) (13). As expected, the inhibitor binds in a deep electropositive cleft where it makes extensive contacts with both the active-site signature sequence (P-loop) and structural determinants that are not present in PTPs. Notably, MIHS binds with the C5 sulfate adjacent to the nucleophilic thiol in contrast to the known specificity of the enzyme for the C3 phosphate of $InsP_6$, suggesting that the binding modes for substrate and inhibitor are distinct.

In this work, we describe high resolution x-ray crystallographic structures of inactive PhyAsr mutants in complex with $InsP_6$ and Ins(1,2,3,5,6)P_5. The PhyAsrC252S·$InsP_6$ complex structure is the first IPPase·$InsP_6$ structure that is consistent with the known substrate specificity of the enzyme. The PhyAsrC252A·Ins(1,2,3,5,6)P_5 complex structure and previous inhibitor structures (13) suggest that IPP substrates have multiple, overlapping binding sites within the binding pocket of the enzyme. To complement the structural studies, fluorescent binding assays were developed and demonstrate that the K_d for $InsP_6$ is several orders of magnitude lower than the apparent K_m

* This work was supported by National Science and Engineering Research Council of Canada (NSERC) discovery grants (to H.-J. W., L. B. S., and S. C. M.) and NSERC studentships (to R. J. G., S. D., and L. M. B.).
[S] This article contains supplemental Fig. S1.
[1] To whom correspondence should be addressed: 4401 University Dr., Lethbridge, AB, Canada T1K 3M4. Fax: 403-329-2057; E-mail: steven.mosimann@uleth.ca.
[2] The abbreviations used are: IPP, *myo*-inositol polyphosphate; 5-IAF, 5-iodoacetamidofluorescein; Ins(1,2,3,5,6)P_5, *myo*-inositol penta*kis*phosphate; $InsP_6$, *myo*-inositol hexa*kis*phosphate; IPPase, inositol polyphosphatase; PhyAsr, *S. ruminantium* IPPase (PhyA); MIHS, *myo*-inositol hexasulfate; PDB, Protein Data Bank; PTP, protein-tyrosine phosphatase; PTPLP, PTP-like phytase.

determined from steady-state kinetic studies. These data suggest that the earliest steps of the PhyAsr reaction mechanism involve an initial substrate binding event followed by a slower catalytic step that may require substrate reorientation. This interpretation is supported by preliminary results from a rapid kinetic study of substrate binding which suggest a multiphasic binding involving, at minimum, a rapid initial phase and another slower phase.

EXPERIMENTAL PROCEDURES

Cloning and Mutagenesis—The pET28b expression construct (13) containing the full-length *S. ruminantium* ORF (minus the putative signal peptide) was used as the template for all cloning and mutagenesis procedures. The signal peptide sequence was determined using SignalP 3.0 (19). PhyAsr numbering begins with 1 at the N terminus of the protein sequence found in GenBank (AAQ13669) including the predicted 27-residue signal peptide. All mutant proteins (C252S, C252A, H188C, and H188C/C252S) were prepared by site-directed mutagenesis using counter-PCR amplification of the expression plasmid as described previously (20). To verify the identity of the construct and the presence of the desired mutations, all PCR products were sequenced at the University of Calgary Core DNA and Protein services facilities. Sequence data were analyzed using the programs SEQUENCHER 4.0 (Gene Codes Corp.) and MacDNAsis 3.2 (Hitachi Software Engineering Co.). All of the primers used in this study were purchased from Integrated DNA Technologies.

Protein Production and Purification—Protein expression was carried out in *Escherichia coli* BL21(DE3) cells (Novagen) for 18 h at 310 K. Cells were grown to an $A_{600\ nm}$ of 0.6–0.8, and protein expression was induced by adding isopropyl-β-D-thiogalactopyranoside to a final concentration of 1 mM. Induced cells were harvested and resuspended in lysis buffer (20 mM KH_2PO_4 (pH 7.0), 300 mM NaCl, 1 mM β-mercaptoethanol), 15 mM imidazole (pH 8.0)). Cells were lysed by sonication, and cell debris was removed by centrifugation at 20 000 × *g*. PhyAsr was purified to homogeneity by metal chelating affinity chromatography (nickel-nitrilotriacetic acid-agarose; Qiagen). Bound protein was washed with lysis buffer and eluted with lysis buffer containing 400 mM imidazole (pH 8.0). PhyAsr was further purified by cation exchange (Macro-Prep High S) and size exclusion chromatography (GE Healthcare, S200). The homogeneity of the purified protein was confirmed by SDS-PAGE (21) and Coomassie Brilliant Blue R-250 staining. Protein (containing an N-terminal His tag) was either used immediately or dialyzed into 20 mM ammonium bicarbonate (pH 8.0) and lyophilized for long term storage.

Crystallization and Ligand Soaking—Crystallization experiments were carried out at room temperature using sitting-drop vapor diffusion with a drop ratio of 2 μl of 20 mg/ml protein solution (in water) to 2 μl of reservoir solution. Crystals were grown in 8–10% PEG 8000, 200–300 mM NaCl, 50 mM sodium acetate (pH 4.8). Ligand solutions were prepared by dissolving $InsP_6$ (Sigma-Aldrich) in mother liquor to a final concentration of 2 mM. Ligand solutions were added to drops containing crystals and incubated for approximately 1 h prior to flash freezing in a solution containing the crystallization reagents, ligand, and 25% glycerol.

TABLE 1
Data collection and refinement statistics for the PhyAsrC252S·$InsP_6$ and PhyAsrC252A·Ins(1,2,3,5,6)P_5 complex structures
Values in parentheses are for the highest resolution shell.

Parameters	PhyAsrC252S·$InsP_6$	PhyAsrC252A·$InsP_5$
Data collection		
Space group	$P2_1$	$P2_1$
a, *b*, *c* (Å)	46.1, 136.9, 79.9	46.0, 137.3, 80.0
β (°)	102.9	103.0
Wavelength (Å)	1.1159	1.1159
Resolution (Å)	51-1.60	37.5-1.55
Observed reflections	560,803	456,682
Unique reflections	120,565	126,093
Completeness (%)	92.9 (77.0)	89.9 (56.8)
Redundancy	4.6 (4.2)	3.6 (2.8)
R_{merge}	0.083 (0.76)	0.074 (0.38)
$I/\sigma I$	10.7 (1.5)	15.5 (2.8)
Refinement statistics		
Resolution (Å)	50-1.60	50-1.55
No. reflections work set	113,134	119,687
No. reflections test set	6,015	6,346
R_{work}/R_{free} (%)	17.0/18.5	16.4/16.9
Asymmetric unit	Dimer	Dimer
Protein atoms	5,103	5,304
Solvent atoms	932	886
Ligand atoms	80	72
Small molecule atoms[a]	47	47
Wilson B (Å^2)	17.9	15.1
Average B protein (Å^2)	16.0	14.6
Average B solvent (Å^2)	30.6	29.3
Average B ligand (Å^2)	39.1	23.2
R.m.s.d.[b] bonds (Å)	0.013	0.011
R.m.s.d. angle (°)	1.66	1.65
Ramachandran distribution		
Most favored (%)	93.1	92.7
Additionally allowed (%)	6.6	6.9
Generously allowed (%)	0.4	0.4

[a] Each structure contains 1 chloride, 4 acetate, and 5 glycerol molecules.
[b] R.m.s.d., root mean square deviation.

Data Collection, Image Processing, and Structure Refinement—Diffraction data (λ = 1.1159 Å) for both complexes were collected at 100 K on beamline 8.3.1 at the Advanced Light Source. Diffraction images were processed with MOSFLM and scaled with SCALA within the CCP4 program suite. Phases derived from the isomorphous D223N structure (Protein Data Bank (PDB) code 2B4P) (13) were used to solve the structures of the PhyAsr ligand complexes. CNS 1.2 (22) was used to refine the models iteratively using simulated annealing and positional and *B*-factor refinement followed by manual model building in XFIT (23). The N-terminal His tag and residues 27–32 lack corresponding electron density and were not included in the final model of either structure. Unless indicated otherwise, figures were prepared with PyMOL (24). Initial topology and parameter files for the ligands were generated using the structure of $InsP_6$ bound to the *E. coli* phytase (PDB code 1DKQ) as a model. For the refinement of the Ins(1,2,3,5,6)P_5 complex, these files were edited to reflect the structures of the ligands. PROCHECK was used throughout refinement to assess the stereochemistry of the model (25). Statistics for the data collection and refinement are presented in Table 1.

Fluorescent Labeling—150 nmol of PhyAsrH188C or PhyAsrH188C/C252S was batch-bound to nickel-nitrilotriacetic acid resin (Qiagen) in binding buffer (20 mM Tris-HCl (pH 8.0), 100 mM NaCl, 10 mM β-mercaptoethanol), and buffer was exchanged with 4 column volumes of labeling buffer (20

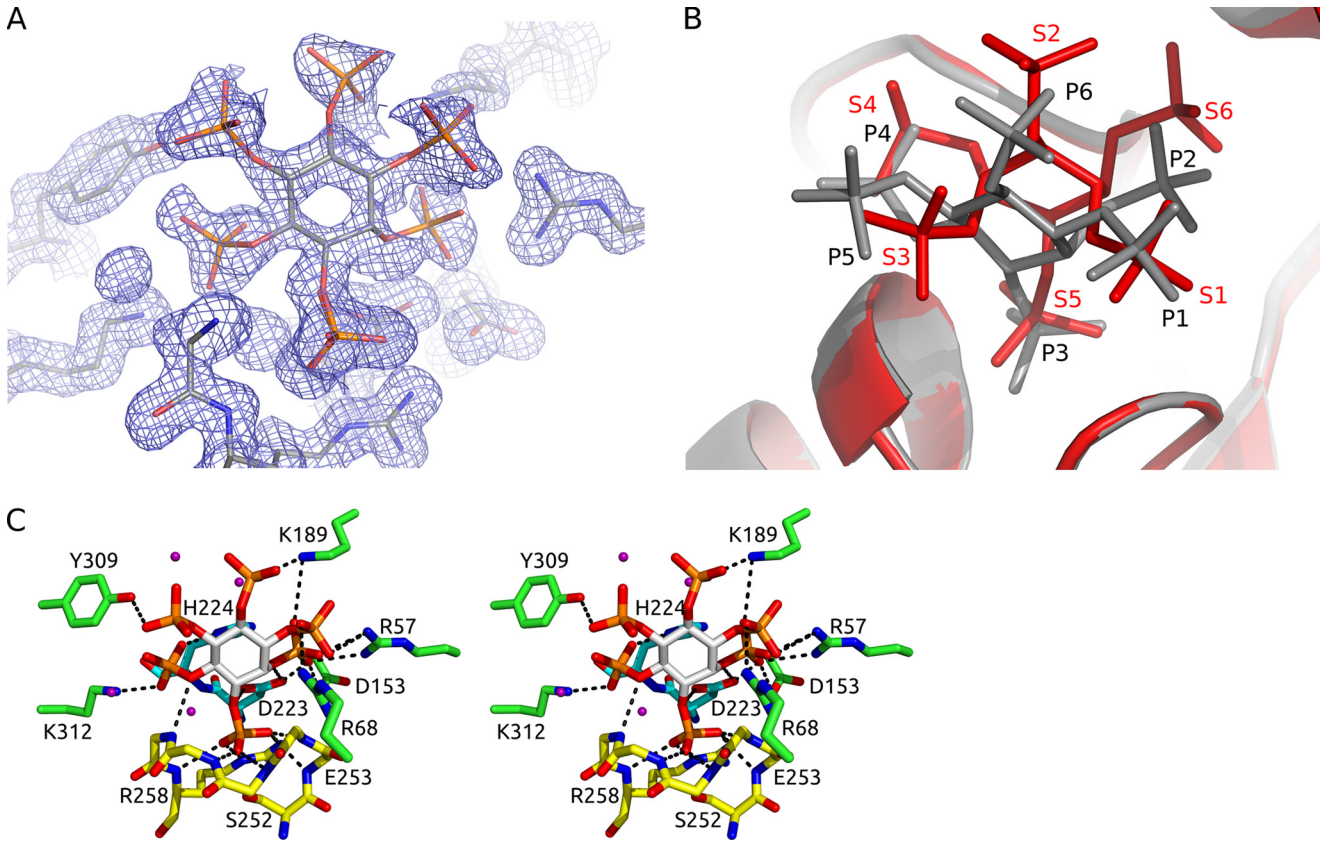

FIGURE 1. **$InsP_6$ ring conformation and electron density.** *A*, $2F_o - F_c$ electron density contoured at 1.5 σ for the $InsP_6$ bound in the active site. *B*, superposition of the PhyAsrC252S·$InsP_6$ complex (*gray*) and the PhyAsr·MIHS complex (*red*; PDB code 1U26). $InsP_6$ binds in a chair conformation with the C2 phosphate in an axial position and the remaining phosphates in equatorial positions. The C3 phosphate is bound in the active site consistent with known specificity of this enzyme. MIHS binds with the C2 phosphate in an equatorial position and with the C5 sulfate in the active site. *C*, divergent stereo view of the interactions between $InsP_6$ and PhyAsrC252S. Residues involved in $InsP_6$ binding are shown as *sticks*, and *dashed lines* represent specific hydrogen bonding or electrostatic interactions. The P-loop (*yellow*) accounts for all backbone contacts with $InsP_6$, whereas the GA loop (*cyan*) and six additional residues (*green*) make direct contacts through their side chains.

mM Tris-HCl (pH 8.0), 100 mM NaCl, 10% glycerol). A 20-fold molar excess of 5-iodoacetamidofluorescein (5-IAF) was added to 2 ml of labeling buffer and incubated with the bound protein for 48 h at 310 K with gentle agitation. The bound protein was washed with labeling buffer until the flow-through was colorless, eluted with elution buffer (20 mM Tris-Cl (pH 8.0), 100 mM NaCl, 2.5 M imidazole (pH 8.0)), and subsequently buffer-exchanged into storage buffer (20 mM sodium acetate (pH 5.0), 300 mM NaCl, 20% glycerol). Labeling efficiencies were ~70%.

Binding Studies—Dissociation constants (K_d) were determined by titrating a fixed amount of 5-IAF labeled PhyAsrH188C/C252S with $InsP_6$. Fluorescence measurements were made using a Cary Eclipse fluorometer (Varian). The 5-IAF fluorophore was excited at 480 nm, and the resulting emission between 490 nm and 550 nm was measured in 0.5-nm increments at a rate of 300 nm/min after a 2-min equilibration. Runs were performed in quadruplicate at 293 K after a 2-min equilibration period following injection of titrant. Blank titrations were performed by titrating 5-IAF-labeled PhyAsrH188C/C252S with buffer. Fluorescent data points were obtained by averaging data from fluorescent emissions across 20 nm, centered on the fluorescence emission maxima (517 nm). The change in fluorescence was obtained by subtracting the blank titrations from the $InsP_6$ titrations. The resulting difference data were evaluated using the following equation,

$$\Delta F1 = 0.5(B_{max}/[P]_t)([P]_t + [L]_t) - (K_d + [P]_t + [L]_t - 4[P]_t[L]_t)^{1/2} \quad \text{(Eq. 1)}$$

where B_{max} is amplitude, $[P]_t$ is the total concentration of PhyAsrH188C/C252S, $[L]_t$ is the total concentration of $InsP_6$/MIHS, and K_d is the dissociation constant (26).

Phosphate Inhibition—PhyAsr (1 μM) was incubated with 2–50 mM $InsP_6$ in the presence and absence of 1.0 and 10.0 mM inorganic phosphate for 5 min, and the products were separated using a CarboPax-100 column (Dionex) following standard protocols (27).

RESULTS

Structure of PhyAsrC252S·$InsP_6$ Complex—To examine the interactions between PhyAsr and its substrate, $InsP_6$, we have determined the high resolution structure (1.6 Å) of the inactive C252S mutant (active-site nucleophile) in complex with $InsP_6$ (PDB code 3MMJ). Analysis of $2F_o - F_c$ omit and difference electron density maps clearly identify density for $InsP_6$ bound in the active site. The $InsP_6$ molecule displays excellent electron density (Fig. 1*A*); however, refinement of the ligand with full occupancy results in negative difference density for all of the

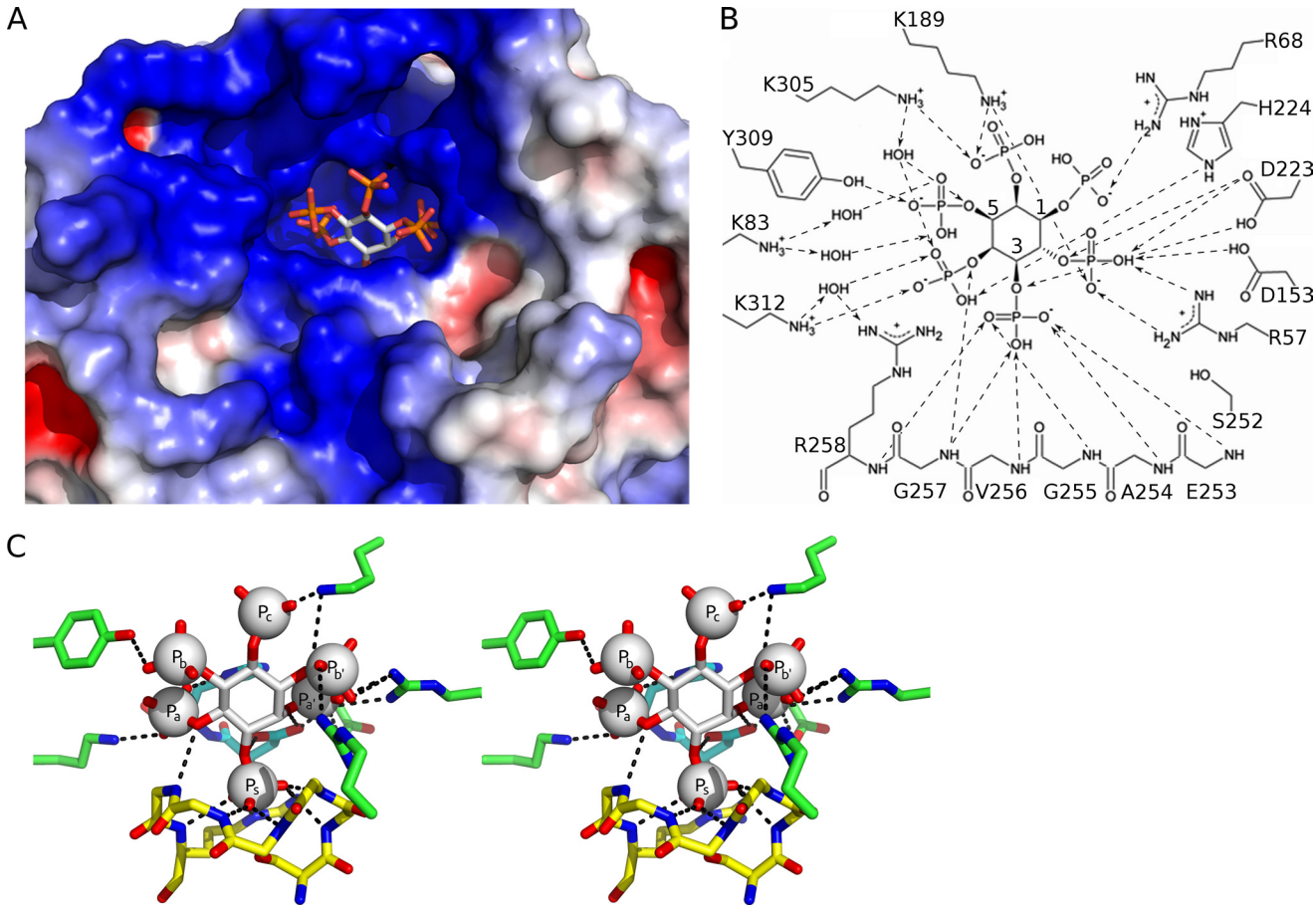

FIGURE 2. *A*, binding of $InsP_6$ to PhyAsrC252S $InsP_6$ binds deep in the highly basic binding pocket. The C5, C6, and C1 phosphates furthest from the scissile phosphoester bond are exposed to bulk solvent. The electrostatic surface potential was calculated using the APBS plugin in PyMOL (24). Positively and negatively charged regions are colored *blue* and *red*, respectively. *B*, schematic is two-dimensional representation of the contacts (*dashed lines*) between PhyAsrC252S and each of the $InsP_6$ phosphates. *C*, divergent stereo view of the interactions between $InsP_6$ and PhyAsrC252S highlights the different phosphoryl group binding sites. The binding sites are labeled P_s, P_a, $P_{a'}$, P_b, $P_{b'}$, and P_c to facilitate discussion of the different ligand binding modes identified in this work.

atoms in the ligand with the exception of the C3 phosphate. To account for this density, we modeled PhyAsrC252S as binding either $InsP_6$ or inorganic phosphate (an impurity in commercial $InsP_6$) with occupancies of 0.75 and 0.25, respectively. Subsequent hydrolysis assays in the presence and absence of inorganic phosphate confirm product inhibition occurs (supplemental Fig. S1) under conditions similar to those used for crystallization and likely accounts for the observed phosphate binding.

In the PhyAsrC252S·$InsP_6$ complex structure, the ligand conformation and orientation are significantly different from previous complex structures with the competitive inhibitor MIHS (13). $InsP_6$ binds to PhyAsrC252S in a chair conformation with the C1 and C3–C6 phosphates in equatorial positions, whereas the MIHS inhibitor was modeled in a chair conformation with only C2 adopting an equatorial position (Fig. 1*B*). As a consequence of this conformational difference, the $InsP_6$ leaving group oxygen of the scissile phosphate is 0.60 Å closer to the general acid (Asp-223) than in the inhibitor complex (12). This was previously predicted from substrate docking studies that suggested an $InsP_6$ conformation similar to that observed in our complex has the lowest conformational energy and the lowest binding energy and positions the leaving group oxygen for protonation by the general acid (13). Next, $InsP_6$ binds to PhyAsrC252S with the C3 phosphate in the active site (Fig. 1*C*) in agreement with the known PhyAsr degradation pathway that shows $InsP_6$ dephosphorylation is initiated at and highly specific for the C3 phosphate (13). Finally, we note that $InsP_6$ binding induces strain in the ligand with the inositol ring adopting a partially twisted chair conformation and increasing the C-O-P angle for the active-site phosphate by 27 degrees relative to the other phosphates. The twisted conformation of the ligand maximizes the agreement with the electron density for the ligand and relieves steric interactions between the general acid loop (Asp-223, His-224) and the C2 phosphate (Fig. 1*C*). Additionally, the increase in the C-O-P angle of the phosphate in the active site relieves steric clashes between the inositol ring and P-loop, specifically Ala-254. This conformation is stabilized by the extensive contacts made to both the C2 phosphate and the scissile phosphate.

$InsP_6$ Contacts with PhyAsrC252S—The binding pocket of PhyAsr is an electropositive cleft that is large enough to accommodate the highly negative $InsP_6$ molecule (Fig. 2*A*). The C3 phosphate is bound adjacent to C252S and positioned for nucleophilic attack. There are extensive contacts between the C2, C3, and C4 phosphates and the protein at the base of the

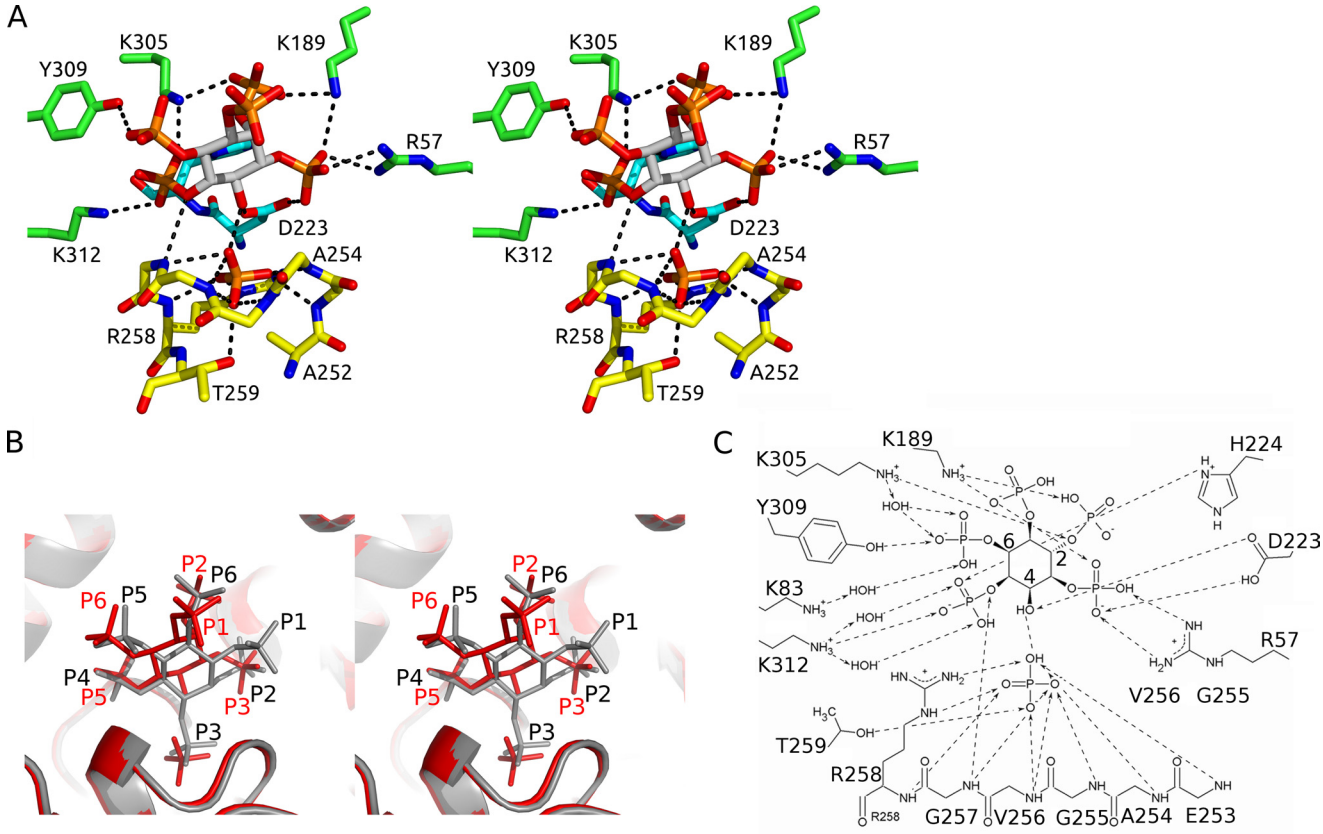

FIGURE 3. **Binding of Ins(1,2,3,5,6)P_5 and inorganic phosphate to PhyAsrC252A.** *A*, divergent stereo view of the interactions between Ins(1,2,3,5,6)P_5, inorganic phosphate, and PhyAsrC252A. Residues contacting the substrate are shown as *sticks* and *colored* as in Fig. 1*C*. Electrostatic interactions and H-bonds are shown as *dashed lines*. *B*, divergent stereo view of the least squares superposition of the PhyAsrC252S·InsP_6 (*gray*) and PhyAsrC252A·Ins(1,2,3,5,6)P_5 (*red*) including the inorganic phosphate bound within the active site. The InsP_5 is rotated and translated away from the P-loop to accommodate the inorganic phosphate. *C*, schematic, two-dimensional representation of the contacts (*dashed lines*) between PhyAsrC252A and each of the Ins(1,2,3,5,6)P_5 phosphates.

binding pocket and relatively few contacts involving the solvent-exposed C1, C5, and C6 phosphates (Fig. 2). Main-chain contacts between PhyAsrC252S and InsP_6 are limited to the scissile C3 phosphate (five contacts) and the adjacent C4 phosphate (one contact). To facilitate the discussion of ligand binding to various IPPs, we will refer to the PhyAsr phosphate binding sites as P_s (scissile phosphate) P_a/$P_{a'}$ (adjacent to scissile phosphate), P_b/$P_{b'}$, and P_c (Fig. 2*c*). Residues that form hydrogen bonds and ion pairs with the substrate are listed in Table 2 and shown schematically in Fig. 2*b*. Ordered solvent molecules are observed coordinating the phosphates in the P_a, $P_{a'}$, and P_b sites. Interestingly, most of the residues involved in binding InsP_6 are also involved in binding MIHS (12) despite the significant conformational differences between ligands. Because there are no significant changes in the main-chain conformation of PhyAsr residues contacting the ligands in the two structures (0.2 Å root mean square deviation for 15 residues), it appears that there are several modes or ways in which the binding pocket can accommodate ligands.

Two notable differences in the binding of InsP_6 and MIHS involve residues Arg-68 and Gly-257. In the absence of substrate and in the MIHS complex structure, the Arg-68 side chain is directed away from the binding pocket and into the solvent. In the InsP_6 complex structure, the Arg-68 side chain undergoes a large, induced-fit movement that brings it into contact with the C1 phosphate. This movement is a result of a large rotation about $\chi1$ and $\chi2$ that shifts the N$\eta1$ and N$\eta2$ atoms of the guanidinium group by to 8.3 and 9.8 Å, respectively. This movement results in the formation of a 3.1 Å contact with the C1 phosphate and may be important for productive substrate binding. Unlike Arg-68, Gly-257 does not change its conformation in the absence of substrate or in the presence of either ligand. Instead, differences in the ligand binding modes give rise to an additional hydrogen bond between the amine of Gly-257 and the bridging oxygen of the C4 phosphate (P_a site) in the InsP_6 complex structure. This hydrogen bond is absent in the inhibitor complex structure and may have a role fixing the orientation of InsP_6 relative to the nucleophile.

Structure of PhyAsrC252A Bound to Ins(1,2,3,5,6)P_5—In an attempt to obtain a structure of the PhyAsrC252A mutant in complex with InsP_6 we unexpectedly observed the binding of Ins(1,2,3,5,6)P_5 and inorganic phosphate (Fig. 3*A*, PDB code 3MOZ). This inositol polyphosphate is a contaminant in commercial InsP_6 purified from plant sources and has previously been observed in the structure of a pleckstrin homology domain soaked with InsP_6 (28). The smaller alanine side chain enables the inorganic phosphate to bind 0.8 Å deeper within the active site than the scissile phosphate of the InsP_6 complex. The binding of inorganic phosphate sterically prevents InsP_6 binding while allowing the binding of Ins(1,2,3,5,6)P_5. The inorganic phosphate in the active site makes a 2.6-Å hydrogen bond with the C4-hydroxyl of Ins(1,2,3,5,6)P_5. The Ins(1,2,3,5,6)P_5 ring

TABLE 2
Contacts (<3.5 Å) in the PhyAsrC252S·$InsP_6$ and PhyAsrC252A·Ins(1,2,3,5,6)P_5 complex structures

$InsP_6$			$InsP_5$		
Residue	Phosphate	Contact	Residue	Phosphate	Contact (Å)
		Å			Å
Arg-57	$P_{a'}$	2.73, 2.88, 2.48	Arg-57	$P_{a'}$	2.91, 3.06, 3.35
Arg-68	$P_{b'}$	3.12			
Asp-153	$P_{a'}$	3.09			
Lys-189	$P_c/P_{a'}$	3.47/3.37	Lys-189	$P_c/P_{a'}$	2.66/3.16
Asp-223	$P_{a'}$	3.10, 2.57, 2.74	Asp-223	$P_a/P_{a'}$	2.63/2.87
His-224	P_a	2.97	His-224	P_a	2.73
Ser-252	P_s	2.50			
Glu-253	P_s	3.00	Glu-253	P_s	2.82
Ala-254	P_s	3.14	Ala-254	P_s	2.96
Gly-255	P_s	2.83	Gly-255	P_s	3.02
Val-256	P_s	2.67	Val-256	P_s	3.17, 2.97
Gly-257	P_a	3.24	Gly-257	P_s/P_a	3.11/3.42
Arg-258	P_s	2.89, 2.87, 2.79	Arg-258	P_s	2.78, 2.83, 2.94
			Thr-259	P_s	2.78
			Lys-305	$P_{b'}/P_a$	2.86/2.71
Tyr-309	P_b	3.26	Tyr-309	P_b	2.60
Lys-312	P_a	2.83	Lys-312	P_a	3.07

adopts a chair conformation similar to the $InsP_6$ ring without the slight twist. However, the ring of Ins(1,2,3,5,6)P_5 is shifted away from the base of the active site by roughly 1 Å and rotated relative to $InsP_6$ (Fig. 3*B*).

PhyAsrC252A contacts with Ins(1,2,3,5,6)P_5 are closely similar to those observed in both the $InsP_6$ and MIHS complex structures despite the differences in ligand orientation within the active site (Table 2). The C3, C5, C6, and C2 phosphates of Ins(1,2,3,5,6)P_5 contact residues that form the $P_{a'}$, P_a, P_b, and P_c sites, respectively, in the PhyAsrC252S·$InsP_6$ complex (Fig. 3, *B* and *C*). The solvent exposed C1 phosphate fails to make direct contacts with PhyAsrC252A whereas the anion makes 10 contacts at the base of the active site, involving main-chain amines of the P-loop and the side chains of Arg-258 and Thr-259.

Based on the shift in the inorganic phosphate position and the smaller size of the alanine side chain, we investigated the possibility that the inorganic phosphate was positioned similarly to the cysteinyl-phosphate intermediate in PTP1B (29). Superposition of the PhyAsrC252A·Ins(1,2,3,5,6)P_5 complex with the PTP1B phosphoenzyme intermediate (PDB code 1A5Y) reveals only small differences in the position of the phosphates that are likely due to the noncovalent nature of the bound inorganic phosphate in our structure (Fig. 4). The similarities suggest the hypothesis is reasonable and the observed contacts between the phosphate anion and PhyAsrC252A will be analogous to those present in a PhyAsr cysteinyl-phosphate intermediate.

$InsP_6$ Binding Studies—To date, the reported binding affinities of phytases for $InsP_6$ or any other inositol phosphates have been based on the Michaelis-Menten kinetic parameter K_m. To examine the K_d of PhyAsr for $InsP_6$ we developed a fluorescent based assay to measure substrate binding. The binding curves obtained for $InsP_6$ are characteristic of a tight binding interaction and indicate that the K_d for $InsP_6$ binding is comparable with, or lower than, the concentration of protein (1 μM) used in the assay (Fig. 5*A*) (30). The sensitivity of our current fluorescent based assay precludes us from significantly decreasing the protein concentration. Although we cannot currently obtain an accurate K_d value, the curve is consistent with PhyAsrC252S having a submicromolar binding affinity for $InsP_6$. In contrast,

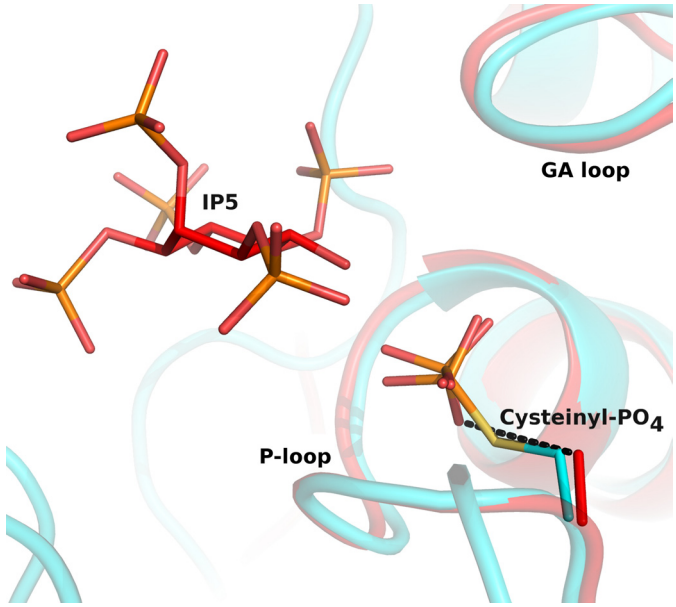

FIGURE 4. **PhyAsrC252A·Ins(1,2,3,5,6)P_5 complex resembles the PTP1B phosphoenzyme intermediate.** Least squares superposition of PhyAsrC252A mutant (*red*) bound to Ins(1,2,3,5,6)P_5 and inorganic phosphate and the phosphocysteine intermediate of PTP1B (*cyan*; PDB code 1A5Y) is shown. The general acid and phosphate binding loops are labeled *GA loop* and *P-loop*, respectively.

K_m values for $InsP_6$ are dependent on ionic strength and vary from 1290 ± 240 μM (100 mM ionic strength) to 150 ± 10 μM (500 mM ionic strength) (31). At all ionic strengths, the K_d for $InsP_6$ determined from the fluorescence binding assay is 2 or more orders of magnitude less than the K_m. These finding suggest that PhyAsr does not utilize a classical Michaelis-Menten reaction mechanism as assumed in previous works.

DISCUSSION

Substrate Conformation—This first structure of a PTPLP in complex with $InsP_6$ has allowed us to identify novel features not observed in the MIHS inhibitor complex. In particular, our PhyAsrC252S·$InsP_6$ structure is consistent with the known $InsP_6$ degradation pathway, positions the leaving group oxygen for protonation by Asp-223 (12), and the $InsP_6$ adopts the energetically preferred ring conformation present under physiolog-

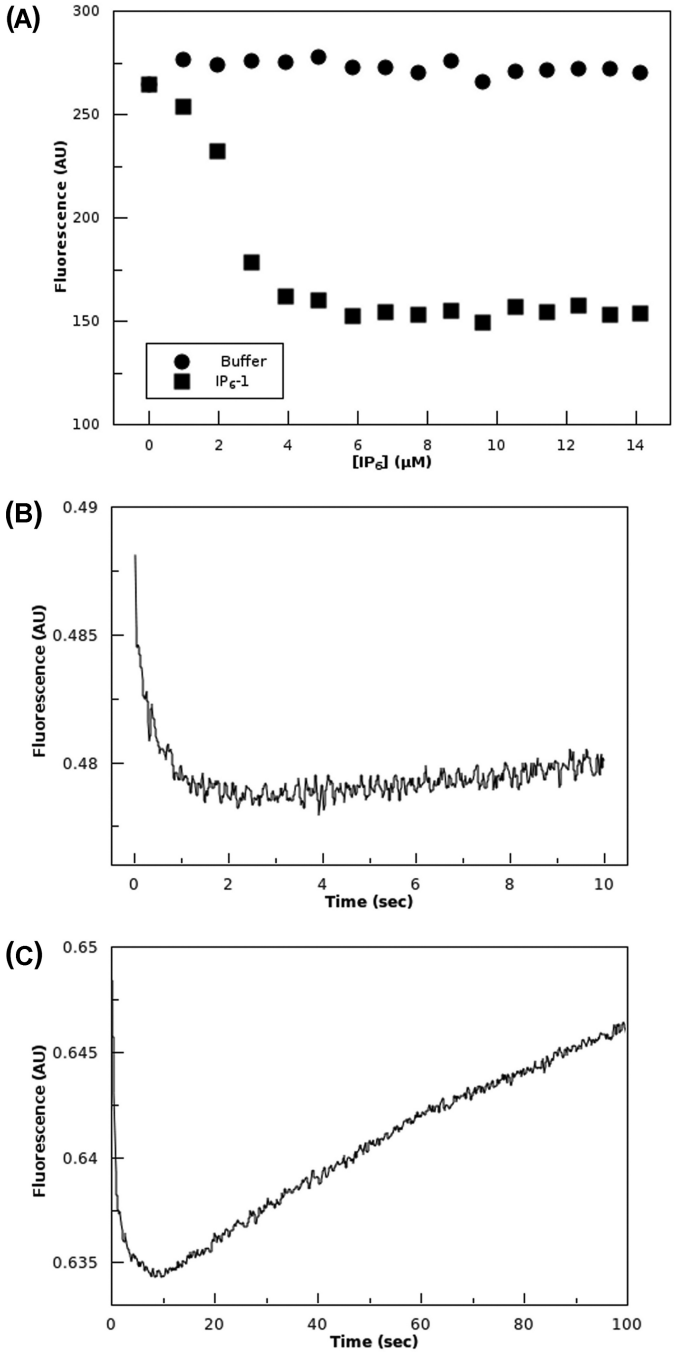

FIGURE 5. **$InsP_6$ binding to PhyAsrH188C/C252S detected by changes in relative fluorescent intensity.** The 5-IAF fluorophore was introduced at the periphery of the active site (H188C) near the P_c site. *A*, titration of PhyAsrH188C/C252S with $InsP_6$. The binding curve suggests a maximal dissociation constant in the low micromolar range. Preliminary rapid kinetics measurements suggest a two-phase binding over 10 s (*B*) and 100 s (*C*).

ical conditions (Fig. 1*C*). In addition, the binding of $InsP_6$ induces strain in the ligand similar to that observed in high resolution structures of several glycosidase and glycosyltransferases (32–34). As a consequence, the substrate adopts a conformation closer to the presumed transition state which minimizes unfavorable steric and electrostatic clashes with the protein while maximizing the stabilizing contacts with the ligand.

In the PhyAsrC252A·Ins(1,2,3,5,6)P_5 complex structure, the observed phosphate anion contacts resemble those of a cysteinyl-phosphate intermediate, whereas the ligand adopts the same energetically preferred ring conformation observed in the PhyAsrC252S·$InsP_6$ complex. However, the Ins(1,2,3,5,6)P_5 is shifted away from the active site. This accommodates the bound phosphate anion and relieves the steric and electrostatic interactions that induce strain in $InsP_6$ (Fig. 2). These observations are consistent with the PhyAsrC252S·$InsP_6$ complex structure representing interactions prior to catalysis and the PhyAsrC252A·Ins(1,2,3,5,6)P_5 structure representing a post-catalytic complex (Fig. 4). Notably, the bound phosphate anion cannot be released from the active site in the observed structure without prior dissociation of the Ins(1,2,3,5,6)P_5 ligand. This agrees with previous findings that clearly indicate that PhyAsr is nonprocessive and releases all products prior to subsequent catalytic cycles (12).

Phosphoryl Group Binding Sites—We have identified several conserved phosphoryl group binding sites (P_a, P_s, and $P_{a'}$) near the base of the active site, and several variable, solvent-accessible binding sites (P_b, P_c, and $P_{b'}$). The P_s site is the catalytic center and as such is directly involved in catalysis. Notably, this site is primarily composed of P-loop residues and accounts for virtually all the main-chain interactions with the Ins(1,2,3,5,6)P_5, $InsP_6$, and MIHS ligands. The P_a and $P_{a'}$ sites (Arg-57, Lys-189, Asp-223, His-224, and Lys-312) are located adjacent to the catalytic site and appear to function as anchor points that ensure the scissile phosphate is correctly oriented for nucleophilic attack. The functions of the variable sites are less clear, but they may be important for binding and discriminating between the lower phosphorylated IPPs that are generated during the degradation of $InsP_6$.

The catalytic properties of several PTPLPs have recently been described (12,16–18), and these enzymes can be separated into high activity and low activity groups. Interestingly, all of the binding residues identified in PhyAsr are conserved in all other high activity PTPLPs whereas the low activity PTPLPs have conservative and nonconservative mutations or deletions at several of these sites. The conservation of these binding residues also appears to play a role in defining substrate specificity because two of the enzymes with mutations to binding residue have significantly altered substrate specificity (16–17, 35).

In each complex structure, residues that form the conserved P_s, P_a, and $P_{a'}$ subsites (Arg-57, Lys-189, Asp-223, His-224, Lys-312, and the P-loop) account for the majority of the contacts to the ligand. In contrast, residues that compose the variable subsites (P_b, P_c, and $P_{b'}$) make relatively few contacts with solvent-exposed phosphoryl groups. Further, there are differences in both the number and nature of the contacts. With the exception of the remote standby site identified by Chu *et al.* (13) the same residues are involved in binding the distinctive Ins(1,2,3,5,6)P_5, $InsP_6$, and MIHS inhibitor conformations. The P_a, $P_{a'}$, and variable subsites are almost exclusively composed of side chains atoms. Consequently, differences of several angstroms in phosphoryl group position can be accommodated by the movement of side-chain atoms without significant main-chain movements.

Arg-68 adopts multiple conformations in the $InsP_6$ complex structure and apparently undergoes a large induced fit movement upon substrate binding and makes a specific contact with the C1 phosphate of $InsP_6$. While this residue is not interacting with Ins(1,2,3,5,6)P_5 substrate it is observed in a closed conformation. In contrast, this residue adopts an open conformation in all PhyAsr structures lacking substrate. Although Arg-68 is not strictly conserved in known PTPLPs, it may participate in substrate binding prior to catalysis, either guiding or orienting the ligand within the PhyAsr active site.

Mechanistic Insight into PhyAsr Catalysis—The K_d values for $InsP_6$ binding (this study) are at least 2 orders of magnitude lower than previously reported K_m values under similar conditions (12, 31). There are several potential explanations for the large, reported K_m values. Based on our structural analysis, binding studies, and the findings of Puhl *et al.* (12) we suggest that a two-step binding mechanism accounts for the discrepancy. Preliminary rapid kinetics data (Fig. 5, *B* and *C*) suggest that binding involves a rapid initial binding of the substrate followed by a slower step. Structural studies clearly indicate that PhyAsr binds substrate or inhibitor in at least three distinct conformations within the electropositive binding pocket. Further, only one conformation ($InsP_6$ complex) is consistent with catalytic competence. We speculate that the rapid initial binding phase represents substrate association with the electropositive binding pocket in one of several conformations followed by a slower phase that results in the substrate adopting a catalytically competent conformation.

To our knowledge, there have been no studies examining the binding of $InsP_6$ to phytases; however, the K_d for the binding of the competitive inhibitor MIHS (K_i) has been determined for both PhyA and PhyB from *Aspergillus ficuum* (36) and PhyA from *Aspergillus fumigates* (37). Interestingly, for each of these enzymes their K_i is at least 1 order of magnitude smaller than their K_m for $InsP_6$. These phytases belong to the histidine acid phosphatase family of phytase and are structurally similar to the *E. coli* phytase. It is not known whether the K_d for the substrate, $InsP_6$, is significantly lower than the K_m for these enzymes. Interestingly, the only other phytate-degrading enzyme that has been structurally characterized in complex with $InsP_6$ is the *E. coli* phytase (PDB code 1DKQ) (14). This enzyme hydrolyzes the C6 phosphate preferentially but was observed to bind the C3 phosphate within the catalytic site. This result suggests that *E. coli* phytase can bind $InsP_6$ in multiple conformations as observed for the PTPLP, PhyAsr. Similar to PhyAsr, the binding pocket of this enzyme is a highly basic cleft that makes extensive contacts with the phosphoryl groups near the catalytic site at the base of pocket.

The discrepancy between the binding affinity of MIHS and the K_m of $InsP_6$ in histidine acid phosphatases, the similarities in substrate binding by PhyAsr and the *E. coli* phytase, and the finding that the *E. coli* phytase can bind $InsP_6$ in multiple conformations, all suggest that histidine acid phosphatases and PTPLPs may both utilize a similar binding mechanism. This mechanism likely involves a rapid initial substrate binding followed by a slower reorientation and may be a general feature of all IPPases.

REFERENCES

1. Irvine, R. F., and Schell, M. J. (2001) Back in the water: the return of the inositol phosphates. *Nat. Rev. Mol. Cell Biol.* **2,** 327–338
2. York, J. D., Odom, A. R., Murphy, R., Ives, E. B., and Wente, S. R. (1999) A phospholipase C-dependent inositol polyphosphate kinase pathway required for efficient messenger RNA export. *Science* **285,** 96–100
3. Hanakahi, L. A., Bartlet-Jones, M., Chappell, C., Pappin, D., and West, S. C. (2000) Binding of inositol phosphate to DNA-PK and stimulation of double-strand break repair. *Cell* **102,** 721–729
4. Chatterjee, S., Sankaranarayanan, R., and Sonti, R. V. (2003) PhyA, a secreted protein of *Xanthomonas oryzae* pv. *oryzae*, is required for optimum virulence and growth on phytic acid as a sole phosphate source. *Mol. Plant Microbe Interact.* **16,** 973–982
5. Macbeth, M. R., Schubert, H. L., Vandemark, A. P., Lingam, A. T., Hill, C. P., and Bass, B. L. (2005) Inositol hexa*kis*phosphate is bound in the ADAR2 core and required for RNA editing. *Science* **309,** 1534–1539
6. Tan, X., Calderon-Villalobos, L. I., Sharon, M., Zheng, C., Robinson, C. V., Estelle, M., and Zheng, N. (2007) Mechanism of auxin perception by the TIR1 ubiquitin ligase. *Nature* **446,** 640–645
7. Majerus, P. W., Zou, J., Marjanovic, J., Kisseleva, M. V., and Wilson, M. P. (2008) The role of inositol signaling in the control of apoptosis. *Adv. Enzyme Regul.* **48,** 10–17
8. Caffrey, J. J., Hidaka, K., Matsuda, M., Hirata, M., and Shears, S. B. (1999) The human and rat forms of multiple inositol polyphosphate phosphatase: functional homology with a histidine acid phosphatase up-regulated during endochondral ossification. *FEBS Lett.* **442,** 99–104
9. Mullaney, E. J., Daly, C. B., and Ullah, A. H. (2000) Advances in phytase research. *Adv. Appl. Microbiol.* **47,** 157–199
10. Rao, D. E., Rao, K. V., Reddy, T. P., and Reddy, V. D. (2009) Molecular characterization, physicochemical properties, known and potential applications of phytases: an overview. *Crit. Rev. Biotechnol.* **29,** 182–198
11. Mullaney, E. J., and Ullah, A. H. (2003) The term phytase comprises several different classes of enzymes. *Biochem. Biophys. Res. Commun.* **312,** 179–184
12. Puhl, A. A., Gruninger, R. J., Greiner, R., Janzen, T. W., Mosimann, S. C., and Selinger, L. B. (2007) Kinetic and structural analysis of a bacterial protein-tyrosine phosphatase-like myo-inositol polyphosphatase. *Protein Sci.* **16,** 1368–1378
13. Chu, H. M., Guo, R. T., Lin, T. W., Chou, C. C., Shr, H. L., Lai, H. L., Tang, T. Y., Cheng, K. J., Selinger, B. L., and Wang, A. H. (2004) Structures of *Selenomonas ruminantium* phytase in complex with persulfated phytate: DSP phytase fold and mechanism for sequential substrate hydrolysis. *Structure* **12,** 2015–2024
14. Lim, D., Golovan, S., Forsberg, C. W., and Jia, Z. (2000) Crystal structures of *Escherichia coli* phytase and its complex with phytate. *Nat. Struct. Biol.* **7,** 108–113
15. Nakashima, B. A., McAllister, T. A., Sharma, R., and Selinger, L. B. (2007) Diversity of phytases in the rumen. *Microb. Ecol.* **53,** 82–88
16. Puhl, A. A., Greiner, R., and Selinger, L. B. (2008) Kinetics, substrate specificity, and stereospecificity of two new protein tyrosine phosphatase-like inositol polyphosphatases from *Selenomonas lacticifex*. *Biochem. Cell Biol.* **86,** 322–330
17. Puhl, A. A., Greiner, R., and Selinger, L. B. (2008) A protein-tyrosine phosphatase-like inositol polyphosphatase from *Selenomonas ruminantium* subsp. *lactilytica* has specificity for the 5-phosphate of *myo*-inositol hexakisphosphate. *Int. J. Biochem. Cell Biol.* **40,** 2053–2064
18. Puhl, A. A., Greiner, R., and Selinger, L. B. (2009) Stereospecificity of myo-inositol hexakisphosphate hydrolysis by a protein tyrosine phosphatase-like inositol polyphosphatase from *Megasphaera elsdenii*. *Appl. Microbiol. Biotechnol.* **82,** 95–103
19. Bendtsen, J. D., Nielsen, H., von Heijne, G., and Brunak, S. (2004) Improved prediction of signal peptides: SignalP 3.0. *J. Mol. Biol.* **340,** 783–795
20. Street, I. P., Coffman, H. R., and Poulter, C. D. (1991) Isopentenyl diphosphate isomerase. Site-directed mutagenesis of Cys139 using "counter" PCR amplification of an expression plasmid. *Tetrahedron* **47,** 5919–5924
21. Laemmli, U. K. (1970) Cleavage of structural proteins during the assembly

of the head of bacteriophage T4. *Nature* **227,** 680–685
22. Brunger, A. T. (2007) Version 1.2 of the Crystallography and NMR system. *Nat. Protoc.* **2,** 2728–2733
23. McRee, D. E. (1999) XtalView/Xfit: a versatile program for manipulating atomic coordinates and electron density. *J. Struct. Biol.* **125,** 156–165
24. DeLano, W. L. (2010) *The PyMOL Molecular Graphics System*, version 1.3r1, Schrödinger, LLC, New York
25. Laskowski, R. A., Hutchinson, E. G., Michie, A. D., Wallace, A. C., Jones, M. L., and Thornton, J. M. (1997) PDBsum: a Web-based database of summaries and analyses of all PDB structures. *Trends Biochem. Sci.* **22,** 488–490
26. Wilden, B., Savelsbergh, A., Rodnina, M. V., and Wintermeyer, W. (2006) Role and timing of GTP binding and hydrolysis during EFG-dependent tRNA translocation on the ribosome. *Proc. Natl. Acad. Sci. U.S.A.* **103,** 13670–13675
27. Greiner, R., Larsson Alminger, M., Carlsson, N. G., Muzquiz, M., Burbano, C., Cuadrado, C., Pedrosa, M. M., and Goyoaga, C. (2002) Pathway of dephosphorylation of *myo*-inositol hexa*kis*phosphate by phytases of legume seeds. *J. Agric. Food Chem.* **50,** 6865–6870
28. Jackson, S. G., Zhang, Y., Haslam, R. J., and Junop, M. S. (2007) Structural analysis of the carboxyl-terminal PH domain of pleckstrin bound to D-*myo*-inositol 1,2,3,5,6-pentakisphosphate. *BMC Struct. Biol.* **7,** 80
29. Pannifer, A. D., Flint, A. J., Tonks, N. K., and Barford, D. (1998) Visualization of the cysteinyl-phosphate intermediate of a protein-tyrosine phosphatase by x-ray crystallography. *J. Biol. Chem.* **273,** 10454–10462
30. Goodrich, J. A., and Kugel, J. F. (2007) Binding and kinetics for molecular biologists, pp. 135–152, Cold Spring Harbor Laboratory, Cold Spring Harbor, NY
31. Gruninger, R. J., Selinger, L. B., and Mosimann, S. C. (2008) Effect of ionic strength and oxidation on the P-loop conformation of the protein-tyrosine phosphatase-like phytase, PhyAsr. *FEBS J.* **275,** 3783–3792
32. Zou, J., Kleywegt, G. J., Ståhlberg, J., Driguez, H., Nerinckx, W., Claeyssens, M., Koivula, A., Teeri, T. T., and Jones, T. A. (1999) Crystallographic evidence for substrate ring distortion and protein conformational changes during catalysis in cellobiohydrolase Ce16A from *Trichoderma reesei*. *Structure* **7,** 1035–1045
33. Davies, G. J., Ducros, V. M., Varrot, A., and Zechel, D. L. (2003) Mapping the conformational itinerary of β-glycosidases by x-ray crystallography. *Biochem. Soc. Trans.* **31,** 523–527
34. Shah, N., Kuntz, D. A., and Rose, D. R. (2003) Comparison of kifunensine and 1-deoxymannojirimycin binding to class I and II α-mannosidases demonstrates different saccharide distortions in inverting and retaining catalytic mechanisms. *Biochemistry* **42,** 13812–13816
35. Gruninger, R. J., Selinger, L. B., and Mosimann, S. C. (2009) Structural analysis of a multifunctional, tandemly repeated inositol polyphosphatase. *J. Mol. Biol.* **392,** 75–86
36. Ullah, A. H., and Sethumadhavan, K. (1998) *myo*-Inositol hexasulfate is a potent inhibitor of *Aspergillus ficuum* phytase. *Biochem. Biophys. Res. Commun.* **251,** 260–263
37. Ullah, A. H., Sethumadhavan, K., Lei, X. G., and Mullaney, E. J. (2000) Biochemical characterization of cloned *Aspergillus fumigatus* phytase (PhyA). *Biochem. Biophys. Res. Commun.* **275,** 279–285